ANNALS OF THE NEW YORK ACADEMY OF SCIENCES
Volume 912

GAS HYDRATES

CHALLENGES FOR THE FUTURE

Edited by
Gerald D. Holder and P. R. Bishnoi

The New York Academy of Sciences
New York, New York
2000

Methane Hydrate Dissociation Rates at 0.1 MPa and Temperatures above 272 K

SUSAN CIRCONE,[a,b] LAURA A. STERN,[b] STEPHEN H. KIRBY,[b]
JOHN C. PINKSTON,[b] AND WILLIAM B. DURHAM[c]

[b]*U.S. Geological Survey, 345 Middlefield Road, MS 977, Menlo Park, California 94025, USA*

[c]*Lawrence Livermore National Laboratory, Livermore, California 94550, USA*

ABSTRACT: **We performed rapid depressurization experiments on methane hydrate under isothermal conditions above 272 K to determine the amount and rate of methane evolution. Sample temperatures rapidly drop below 273 K and stabilize near 272.5 K during dissociation. This thermal anomaly and the persistence of methane hydrate are consistent with the reported recovery of partially dissociated methane hydrate from ocean drilling cores.**

INTRODUCTION

Naturally occurring sI methane hydrate has been recovered from numerous ocean drill cores in a partially dissociated state. Retrieved cores can contain several phases: hydrate, fine-grained sediment with altered textures, saline pore water that has been freshened by hydrate dissociation, methane gas in excess of *in situ* saturation levels, and occasionally ice. Drill core temperatures measured after recovery are depressed several degrees below the baseline core temperature in zones observed or inferred to contain gas hydrate.[1–3] Temperatures can be depressed as much as 2 K below the H_2O melting point at 273.15 K and are lower than any encountered during core recovery.[1,2] Such thermal anomalies have been attributed to the endothermic enthalpy of hydrate dissociation. An experimental study on synthetic methane hydrate dissociation at temperatures above 272 K may provide insights into these observations.

Moreover, temporary preservation of hydrate has been observed below 273 K and at 0.1 MPa, first noted in sI methane deuteriohydrate[4] and later in sI methane hydrate at high levels (more than 50% of the sample),[5,6] as well as in sII natural gas hydrates.[7] In experiments performed between 204 and 270 K,[6] we observe highly suppressed dissociation rates between 250 and 270 K, and 50–90% of the hydrate remains preserved after 24 hours, based on CH_4 evolution and X-ray diffraction analysis of samples. In contrast, below 250 K the time to 50% dissociation is several orders of magnitude smaller. We were interested in investigating methane hydrate dissociation kinetics at temperatures above 270 K following rapid depressurization to 0.1 MPa to better define the regime of anomalous preservation observed at lower temperatures.

[a]Telecommunication. Voice: 650-329-5674; fax: 650-329-5163.
scircone@isdmnl.wr.usgs.gov

The purpose of our study was fourfold: (1) to determine the dissociation rates of methane hydrate above 270 K, (2) to profile sample temperature during dissociation, (3) to identify factors that control dissociation rates in this temperature regime, and (4) to begin a preliminary investigation of the effects of natural impurities (sediment and sea water) on hydrate dissociation.

EXPERIMENTAL METHOD

Hydrate Synthesis

Polycrystalline methane hydrate, with expected stoichiometry $CH_4 \cdot 6.1\ H_2O$, was synthesized from granular water ice and pressurized CH_4 using the method of Stern *et al.*[8] Samples had at most trace amounts of ice remaining after synthesis and a porosity of about 30%. The 30 g hydrate samples were cylinders, 2.54 cm in diameter and approximately 9.3 cm in length. The sample axis was held vertical during synthesis and dissociation (see FIGURE 1).

Modifications were made to the hydrate synthesis procedure for several samples. A hydrate/sediment aggregate was made by mixing 150 ± 50 μm quartz sand with the ice (volume ratio 3:7) prior to synthesis. After synthesis, methane pressure (P_{CH_4})was reduced to 4–5 MPa and temperature was held near 275 K. Sea water (SMOW) pressurized with CH_4 to above 10 MPa was introduced through a port above the sample and partially permeated the samples by gravity. The samples were annealed at 276 ± 1 K, 10 MPa for three days prior to dissociation. Additional hydrate growth did occur based on analysis of identically treated samples.

Dissociation Procedure

(1) Maintaining high P_{CH_4}, each sample was equilibrated at a temperature between 272 and 289 K by immersing the pressure vessel in a heated ethanol bath inside a freezer (FIG. 1). (2) P_{CH_4} was reduced over several minutes to at least twice the equilibrium pressure. (3) Sample vessels were rapidly depressurized to 0.1 MPa in about 15 s and then opened to the flow meter. This depressurization rate is an upper limit of the pressure–time pathway encountered during core retrieval. (4) Internal sample temperatures were monitored with one to four thermocouples, and CH_4 evolution was monitored with a custom-built flow meter (see FIG. 1). The external bath temperature (T_{ext}) was held constant during dissociation.

Temperature Measurement

Both T_{ext} and internal sample temperatures were monitored during dissociation (FIG. 1, left). T_{ext} was measured with an RTD located near the vessel. Sample temperatures were monitored using one of two setups. In setup #1, three thermocouples were located along the cylinder axis at the sample top (8.9 cm from sample bottom), middle (4.7 cm), and bottom (0.6 cm). The side thermocouple (4.8 cm) is a few mm in from the sample surface. In setup #2, two thermocouples were located along the cylinder axis, one about 0.5 cm into the sample top and the other 3.5 cm up from the

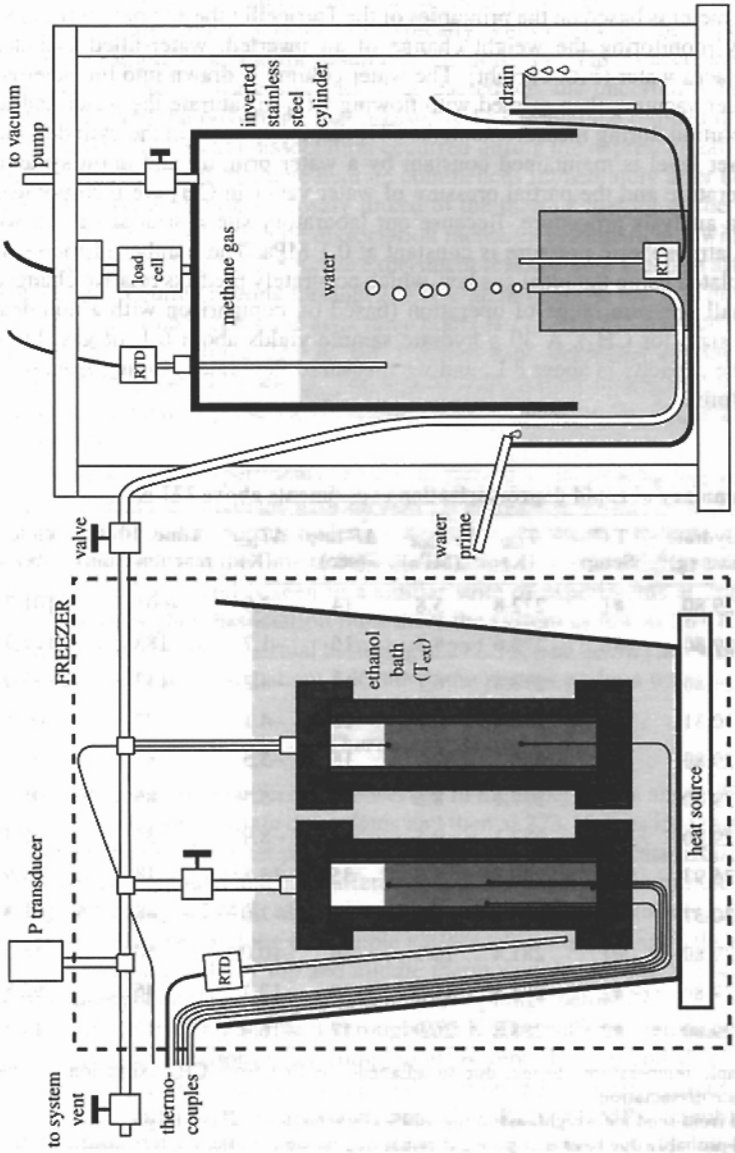

FIGURE 1. Schematic diagram (not to scale) of experimental apparatus showing sample thermocouple configurations used to monitor thermal evolution (*left*) and the custom-built flow meter that measures the amount of evolved CH_4 (*right*) during dissociation. Thermocouples, RTDs, load cell, and pressure transducer are interfaced with a data acquisition system.

bottom. The K-type thermocouples measured within ±0.1 K of 273.15 K in an ice/water calibration bath.

Custom-Built Flow Meter

The flow meter is based on the principles of the Torricelli tube and determines gas flow rate by monitoring the weight change of an inverted, water-filled cylinder as CH_4 displaces water (FIG. 1, right). The water column is drawn into the inverted cylinder under vacuum, then primed with flowing CH_4 to saturate the water and to minimize solution during measurement. As CH_4 displaces water in the cylinder, the external water level is maintained constant by a water priming and drain system. Water temperature and the partial pressure of water vapor in CH_4 are incorporated into the data analysis procedure. Because our laboratory site is near sea level, we assume that atmospheric pressure is constant at 0.1 MPa. The number of moles of CH_4 is calculated using the ideal gas law, which accurately predicts relative changes over the small pressure range of operation (based on comparison with a nonideal equation of state for CH_4). A 30 g hydrate sample yields about 6 L of gas. Flow meter volume capacity is about 8 L, and we measured flow rates ranging from 0.01 to 3,000 ml/min.

TABLE 1. Summary of rapid depressurization experiments above 272 K

Sample ID	Hydrate mass (g)[b]	T.C. Setup	T_{init} (K)	P_{init} (MPa)	ΔP rate (sec)	ΔT_{init}[a] (K)	Time, 100% reaction (min)	Yield (%)
C126	29.80	#1	272.8	5.8	14	−3.9	>605	101.7
C83	29.80	#2	273.6	9.3	16	−1.7	183	122.3[c]
C118	29.80	#1	273.8	6.1	12	−4.2	147	103.0
C77	30.31	#2[d]	276.4	9.3	12	−4.1	72	100.5
C114	29.80	#1	276.5	7.9	18	−5.5	85	96.0
C122	29.80	#1	277.1	8.5	12	−5.5	86	95.6
C129	29.80	#1	277.3	9.5	22	−8.9	35	125.3[e]
C130	26.93	#2[f]	277.3	7.6	35	−13.8	18	63.9[g]
C78	30.37	#2[f]	279.1	9.5	12	−7.0	48	101.3
C116	29.80	#1	281.4	10.1	16	−10.0	50	86.0
C81	29.80	#2	283.8	15.6	19	−12.1	46	96.8
C86	29.80	#2	288.8	26.9	17	−16.4	17	119.3[c]

[a]Initial sample temperature change, due to adiabatic cooling from CH_4 expansion and the onset of hydrate dissociation.

[b]Calculated from seed ice weight, assuming 100% conversion to $CH_4 \cdot 6.1H_2O$.

[c]High yield probably due to excess pore gas remaining in sample after depressurization step.

[d]Only one thermocouple, in top position.

[e]Hydrate sample contained added sea water. High yield due to hydrate growth from sea water.

[f]Only one thermocouple, in middle position.

[g]Hydrate/sediment aggregate with sea water added. Low total is due to the longer depressurization step, in which the vented gas included that from hydrate dissociation.

RESULTS

Rates of Dissociation

A summary of the rapid depressurization experiments above 272 K is listed in TABLE 1. Methane gas yields are typically within ±5% of the expected values (based on sample mass and the assumed stoichiometry). This is acceptable given the possible presence of trace amounts of unreacted ice, the uncertainty in expected n (6.1 ± 0.1), and the possibility that pressurized gas remained trapped in pores (high yield) and/or that partial dissociation occurred during the depressurization step (low yield). Breakdown of methane hydrate commences immediately after depressurization, and CH_4 evolution is closely linked to the thermal history of the sample (see FIGURE 2). The rate of hydrate dissociation increases systematically with increasing T_{ext} (see FIGURE 3). At 272.8 K, the experiment reached 80% reaction after 10 hours. The sample required heating through 273 K to achieve 100% reaction in a reasonable time. Dissociation is complete after three hours at 273.6 to 273.8 K and only 18 minutes at 288.8 K. Above 273 K, the reaction time decreases exponentially with increasing T_{ext} (see FIGURE 4). The significantly longer reaction time at 272.8 K links the anomalous preservation region at 250–270 K[6] to the $T_{ext} > 273$ K region explored here.

Reconnaissance experiments (TABLE 1) show that introducing impurities significantly increases the methane hydrate dissociation rate at about 277 K (FIG. 4). Rates increase in the order: porous hydrate < hydrate + sea water < hydrate + quartz sand + sea water, such that the time to 80% dissociation is four and thirteen times shorter, respectively. This trend is seen in a similar suite of experiments at 268 K (unpublished data). Higher dissociation rates drive the system as low as 263 K in the sediment/sea water sample, thermal buffering at 272.5 K (see below) is not observed, and H_2O melting is depressed about 2 K due to the presence of sea water.

Thermal Buffering

Two-stage thermal buffering is observed in the experiments above 272 K, first at 272.5 K as methane hydrate dissociates and then at 273.15 K as ice reaction product melts (see FIGURE 5). After plummeting below 273 K on depressurization, temperatures partially rebound and are buffered at 272.5 ± 0.2 K within minutes, regardless of T_{ext}. When $T_{ext} < 274$ K, all thermocouples record thermal buffering, although the effect later disappears along the sample surface while continuing in the interior. The effect is observed only by top and middle thermocouples for $T_{ext} > 274$ K. Side and bottom thermocouples show that temperatures plunge below 273 K after depressurization, then climb steadily back through 273 K. The buffering temperature is maintained until dissociation nears completion, is reproducible and distinct from the buffering at the H_2O melting point, and is observed in other hydrate dissociation experiments (heating from low T through 273 K at 0.1 MPa, unpublished data). The buffering temperature is not constant, increasing very slowly over time from 272.3 to 272.7 K during dissociation. Peters *et al.*,[9] observe similarly depressed temperatures between 272 and 273 K in their experiments. Thermal buffering at the ice point may continue after dissociation is complete, indicating the presence of an H_2O ice/water mixture. After dissociation ceased, vessels were opened in

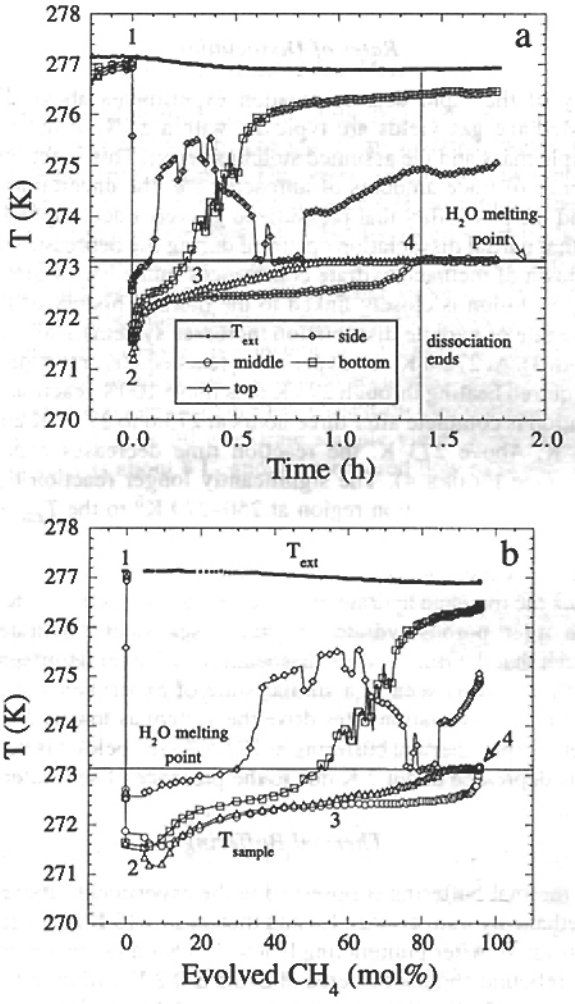

FIGURE 2. Thermal history (**a**) and CH_4 evolution (**b**) of a dissociating methane hydrate sample at 277 K (Run C122, see TABLE 1). T_{ext} remains approximately constant. *Point 1*: at time = 0, internal sample temperature and T_{ext} are nearly isothermal. Pressure is then dropped to 0.1 MPa (see text). *Point 2*: sample temperatures plunge within seconds to a minimum below 273 K. As dissociation proceeds, the sample temperature is buffered at about 272.5 K (top and middle thermocouples). Temperature evolves continually at the bottom and side thermocouple locations as CH_4 evolves and ice (reaction product) melts. *Point 3*: temperatures at the top and middle begin to diverge as dissociation nears completion at the sample top. *Point 4*: as dissociation ends, the sample interior warms above 272.5 K. In the four-thermocouple experiments, the top and middle thermocouples are buffered at the ice point of 273.15 K until the ice melts. Only every fourth point has been plotted for symbol clarity.

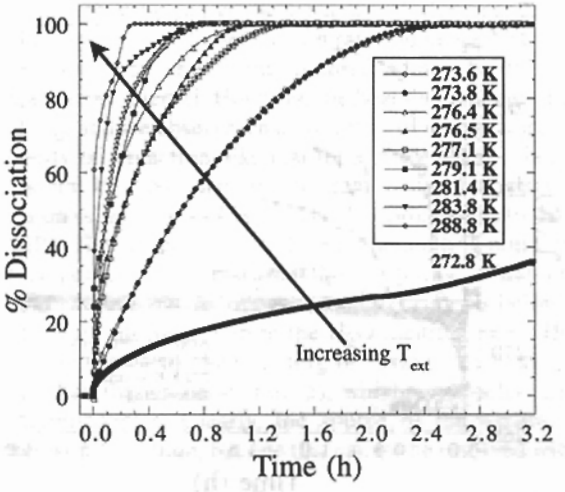

FIGURE 3. Methane evolution with time for all experiments, showing that dissociation rates systematically increase with increasing T_{ext}. Percent dissociation (the extent of reaction) is the measured amount of CH_4 normalized to the expected amount. Note the reproducibility between the two experiments conducted at 273.7 ± 0.1 K. Every fifth point has been plotted.

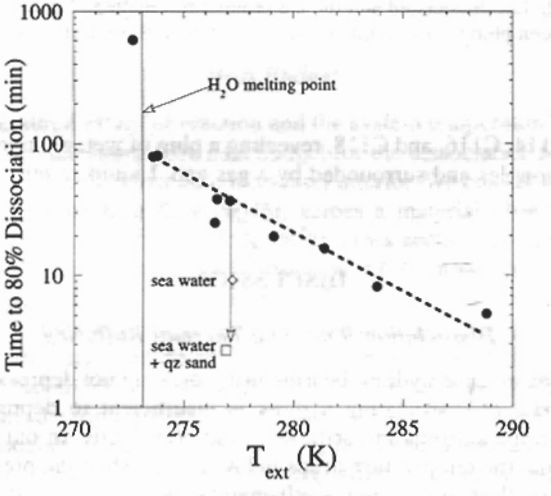

FIGURE 4. The exponential effect of T_{ext} on the time elapsed for 80% dissociation of the hydrate to occur. The scatter in the data is likely due to minor differences in the depressurization procedure. In the early experiments, depressurization was more rapid (under 10 sec) and involved a larger pressure drop (more than twice the equilibrium pressure). This difference appears to produce dissociation rates that are initially slightly higher than those in our later experiments. Curves for 90, 95, and 100% dissociation (not shown) are shifted up in time but have similar slopes. Preliminary results for hydrate + sea water and hydrate/sediment aggregate + sea water samples at about 277 K show the compounding effect of adding impurities (indicated by the *arrow*).

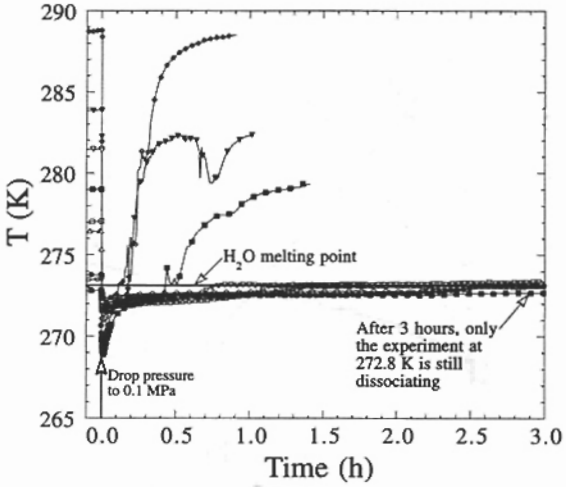

FIGURE 5. Thermal histories recorded by the middle thermocouples, showing the two-stage thermal buffering at 272.5 ± 0.2 K and 273.15 K (see text). Top thermocouples (not shown) record a similar history. The initial sample temperature is seen to the left of time 0, and is isothermal with T_{ext} at the start of rapid depressurization. The minimum T depends on the depressurization procedure and initial dissociation rates. After the material surrounding the thermocouple has dissociated and the ice product has melted, T rises toward T_{ext}. Every fifth point has been plotted, and symbols are equivalent to those in FIGURE 3.

experiments C114, C116, and C118, revealing a plug of wet, granular ice around the center thermocouples and surrounded by a gas gap. Liquid water had pooled at the vessel bottom.

DISCUSSION

Dissociation Rates and Thermal Buffering

Temperatures in some hydrate-bearing drill cores are not depressed below 273 K because the mass of dissociating hydrate is insufficient to depress temperatures to this extent in the surrounding sediments and pore fluids. In our experiments on methane hydrate, the temperature drops below 273 K when the pressure is reduced to 0.1 MPa, regardless of T_{ext}, and is self-maintained at not more than 272.7 K until the dissociation reaction nears completion (above 95%). This thermal buffering effect occurs in actively dissociating parts of the samples. When $T_{ext} > 274$ K, neither buffering at this temperature nor at the ice point occurs along the side or bottom surfaces. The sample dissociates and the ice product melts preferentially and quickly along these surfaces. Dissociation rates are increased significantly by impurities present in natural systems. The effect of sea water may be extreme in our experiments because of the high sample porosity and the high thermal conductivity of sea water relative to CH_4. A detailed study of the effects of impurities is in progress.

A key question arises: what causes the thermal buffering near 272.5 K? An apparent buffering effect could occur if the reaction rate and hence heat consumption rate were balanced by the heat flux rate from the surroundings, holding the sample temperatures within a narrow interval. However, the heat flux and buffering temperature should vary with T_{ext}, and we observe a narrow range of temperatures. It is more likely a thermal property of a reaction, like that for a phase change, but what that reaction might be is unclear. No methane hydrate phase boundary, including the metastable extension of hydrate $\rightarrow CH_4 + H_2O(l)$, corresponds to the buffering temperature at 0.1 MPa. The temperature is close to the melting point of H_2O, a correspondence that is probably not coincidental. Buffering is not observed in the isothermal portions of the rapid depressurization experiments below 272 K,[6] where experimental conditions are farther from the H_2O melting curve. However, we are not observing a simple case of H_2O melting or fusion: the buffering temperature is markedly lower than the ice point (FIG. 5), which is recorded after dissociation ceases at the thermocouples. Clearly, the source of the narrow buffering near 272.5 K is an interesting question, but one that cannot be resolved with the data from this study.

Although the values of the isothermal T_{ext} span 16 K, all of the reactions proceed at the same temperature after a few minutes of dissociation. However, the rate of dissociation increases monotonically with T_{ext}. We infer that the rate is a function of the heat flow supplied from the surroundings (bath) into the sample through the vessel. This influx supplies heat for the endothermic hydrate dissociation reaction. In the next section, we compare the cumulative heat budget for dissociation and the calculated heat flow into the system.

Heat Budget

Using the measured extent of reaction and the system temperature evolution over time, we calculated the cumulative heat budget for the dissociation reaction and the expected heat flow from the bath into the vessel interior. We considered the simplest problem of steady-state heat flow, $\Delta Q/\Delta t$, across a material (304 stainless steel) with thermal conductivity k (0.3 J/sec·K·cm[10]), cross section A (area of vessel surface), thickness Δx, and temperature difference ΔT (sample temperature $- T_{ext}$), where $\Delta Q/\Delta t = -kA(\Delta T/\Delta x)$. We assumed that the vessel wall is continuous and that the indium jacket lining the sample has no significant effect. We ignored vessel wall curvature, using the inner and outer wall surface areas as boundary conditions. We considered only radial heat flow through the vessel sides or axial heat flow through the vessel bottom (the top is insulated by a layer of CH_4). The heat budget for methane hydrate dissociation was calculated using the starting amount of hydrate, the enthalpy of dissociation (18.13 kJ/mol for $CH_4 \cdot 6H_2O$[11]), and the reaction progress with time (FIG. 3).

The calculated total radial heat flow (vessel sides) by the end of hydrate dissociation exceeds that needed to dissociate the hydrate by more than 50-fold (see FIGURE 6). There would be *ample* heat to also melt 100% of the ice product by the end of dissociation, but this is not observed experimentally. Axial heat flow (vessel bottom) is comparable to that needed to dissociate hydrate on the reaction time scale (FIG. 6). At 273.8 K, the calculated heat flow is insufficient for complete dissociation. In higher temperature experiments, heat flow lags behind heat consumption for

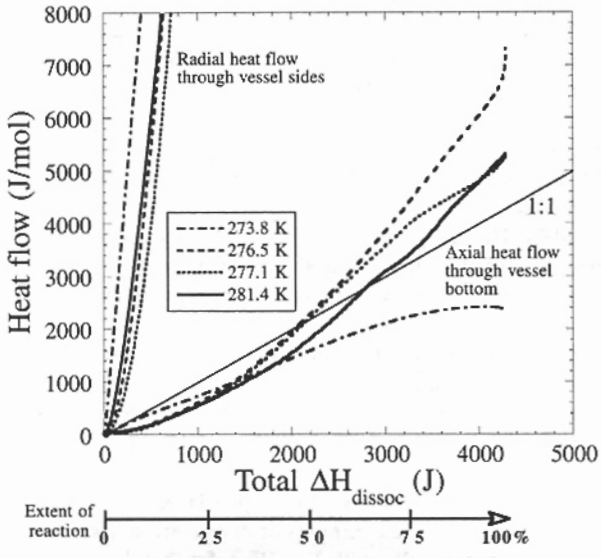

FIGURE 6. Comparison of the cumulative heat needed to dissociate hydrate near 272.5 K and the calculated heat flow through the vessel from the surroundings (ethanol bath) into the samples. Radial heat flow moves heat too quickly into the sample: dissociation should be finished in minutes and all ice should be melted at the end of the experiments, both predictions inconsistent with observations (see text). Axial heat flow is more consistent with observed dissociation rates (see text). Note that curves were placed at the lower bound (heat flow based on the inner stainless steel surface area) for the radial heat flow results; heat flow would be slightly higher for a true cylindrical conduction model. The samples are believed to be largely insulated from radial heat flow by a gas layer (see text and FIG. 7c).

about 50% of the reaction. At the end of dissociation, however, the available excess heat is sufficient to melt 10–30% of the ice product, consistent with observed vessel contents.

Of course, both radial and axial heat flow occurred in the experiments. The calculations can be reconciled by using the thermal evolution data (see FIGURE 7). In warmer tests, sample temperatures near the cylinder surface exceeded 273 K in minutes. Thus, this zone was hydrate- and ice-free, leaving only CH_4 and H_2O (l) (FIG. 7c). The water segregated by gravity, leaving CH_4 along the sides. Methane gas has a thermal conductivity 0.1% that of stainless steel.[10] As the gap between the steel and sample exceeds 13 μm, CH_4 becomes an insulating layer and greatly reduces the radial heat transfer. The pooling water is a better conductor (2% that of stainless steel[10]), although heat transfer will be affected when the water depth exceeds 0.5 mm. In the 273.8 K experiment, radial heat flow occurred over a longer time interval, since the side and bottom thermocouples indicated that hydrate and/or ice was present along the sample perimeter throughout the reaction (FIG. 7b). These observations are broadly consistent with the independent results of Peters *et al.*[9]

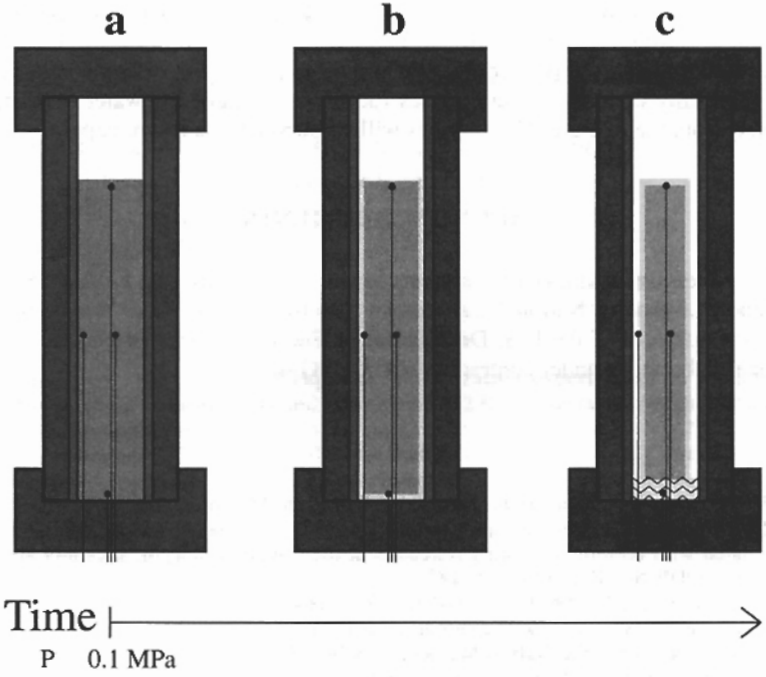

FIGURE 7. Schematic diagram of sample assembly, phases, and their distribution as dissociation proceeds: stainless steel synthesis/reaction vessels (*dark gray*), sample (□, CH_4; ■, hydrate; ▨, H_2O [s→l]; ▩, H_2O [l]), and thermocouples (positions shown). Diagrams are approximately to scale. **(a)** Prior to depressurization: $T_{hydrate} = T_{ext}$, porous hydrate + CH_4. **(b)** After depressurization: $T < 273$ K, hydrate + CH_4 + H_2O (s→l). Dissociation is greater along sample sides and bottom, and ice product may begin to melt. **(c)** Several minutes after depressurization ($T_{ext} > 274$ K): $T_{side,\ bottom} > 273$ K, $T_{top,\ middle} \approx 272.5$ K, hydrate + CH_4 + H_2O (s→l). An insulating CH_4 gap has formed and H_2O (l) pools at the vessel bottom (see text). A similar configuration is observed after dissociation ceases, when only melting ice remains around the center thermocouples (see text).

Their vessel axis was horizontal, and they observed preferential ice melting and water pooling along the bottom surface, clearly indicating that the direction of maximum heat flow was perpendicular to the vessel axis over a narrow, lower sector of the vessel circumference for the latter part of the experiment.

CONCLUSIONS

Temperature depression below 273 K has been observed in hydrate-bearing ocean drilling cores, suggesting that the process observed in our experiments is similar to that occurring in the field. A significant finding of our study is that at temperatures relative to natural settings, hydrate dissociation is a thermal process that is largely

dependent on the heat flow into the system. Our results may help improve procedures for natural hydrate sample recovery. For instance, core retrieval systems could reduce heat flow into the drill core by using insulating gas gaps or by segregating the more thermally conductive fluid phases (pore water and/or the water dissociation product) from the hydrate. These issues will be pursued in a future paper.

ACKNOWLEDGMENTS

We gratefully acknowledge support by a grant from the LDRD Program, Lawrence Livermore National Laboratory, Livermore, CA. Work was performed under the auspices of the U.S. Department of Energy by the Lawrence Livermore National Laboratory under contract W-7405-ENG-48.

REFERENCES

1. WESTBROOK, G.K. *et al.* 1994. Proc. ODP, Init. Rep. **146:** 611.
2. KASTNER, M. *et al.* 1995. Relation between pore fluid chemistry and gas hydrates associated with bottom-simulating reflectors at the Cascadia Margin, sites 889 and 892. Proc. ODP, Sci. Res. **146:** 175–187.
3. PAULL, C.K. *et al.* 1996. Proc. ODP, Init. Rep. **164:** 623.
4. DAVIDSON, D.W. *et al.* 1986. Laboratory analysis of a naturally occurring gas hydrate from sediment of the Gulf of Mexico. Geochim. Cosmochim. Acta **50:** 619–623.
5. YAKUSHEV, V.S. & V.A. ISTOMIN. 1992. Gas-hydrates self-preservation effect. *In* Physics and Chemistry of Ice. N. Maeno & T. Hondoh, Eds.: 136–140. Hokkaido University Press, Sapporo.
6. STERN, L.A. *et al.* 1998. Thermal decomposition of methane hydrate at 0.1 MPa: short-term preservation by rapid depressurization. EOS Trans. AGU **79:** 462.
7. GUDMUNDSSON, J.S. *et al.* 1994. Storing natural gas as frozen hydrate. SPE Prod. and Fac. 69–73.
8. STERN, L.A. *et al.* 1996. Peculiarities of methane clathrate hydrate formation and solid-state deformation, including possible superheating of water ice. Science **273:** 1843–1848.
9. PETERS, D.J. *et al.* 2000. Hydrate dissociation in pipelines by two-sided depressurization: experiment and model. Ann. N.Y. Acad. Sci. **912:** this volume.
10. WEAST, R.C. 1985. CRC Handbook of Chemistry and Physics. CRC Press, Inc., Boca Raton.
11. HANDA, Y.P. 1986. Compositions, enthalpies of dissociation, and heat capacities in the range 85 to 270 K for clathrate hydrates of methane, ethane, and propane, and enthalpy of dissociation of isobutane hydrate, as determined by a heat-flow calorimeter. J. Chem. Thermodyn. **18:** 915–921.